JOURNAL OF APPLIED PHYSICS VOLUME 90, NUMBER 3 1 AUGUST 2001

Monte Carlo analysis of the noise behavior in Si bipolar junction transistors and SiGe heterojunction bipolar transistors at radio frequencies

M. J. Martín-Martínez,[a] S. Pérez, D. Pardo, and T. González
Departamento de Física Aplicada, Universidad de Salamanca, Plaza de la Merced s/n, 37008 Salamanca, Spain

(Received 29 November 2000; accepted for publication 11 May 2001)

We present a comparative analysis of the current spectral densities in a Si bipolar junction transistor (BJT) and a SiGe heterojunction bipolar transistor (HBT) of identical geometry performed by means of an ensemble Monte Carlo simulator self consistently coupled with a two-dimensional Poisson solver. We focus on the physical origin of the different noise sources in the transistors at rf when varying the injection level conditions. At low injection the spectral density of base current fluctuations, $S_{\rm JB}(0)$, is governed by thermal noise related to the base resistance, while the collector spectral density, $S_{\rm JC}(0)$, reaches a typical shot noise response. At high current density the onset of high injection in the base and the base push-out play an important role in the noise behavior of both transistors. Thus, $S_{\rm JC}(0)$ deviates from the typical shot noise response. Hot carrier effects are also present. In the HBT, these effects are less important than in the BJT due to the SiGe/Si heterointerface, and $S_{\rm JB}(0)$ can be neglected in the overall noise analysis because of the Ge content benefits when the structure enters the high-injection regime. © *2001 American Institute of Physics.*
[DOI: 10.1063/1.1384850]

I. INTRODUCTION

The silicon–germanium heterojunction bipolar transistor (HBT) is the first practical band gap-engineered device to be realized in silicon. SiGe HBTs technology is poised for entering the commercial rf and microwave market offering many performance advantages over Si bipolar junction transistors (BJTs), including higher values of common-emitter dc-current gain (β) and transition frequency (f_T),[1] together with excellent minimum noise figures or $1/f$ noise corner frequencies below 500 Hz.[2] Their excellent broadband noise characteristics make these devices powerful for modern communication systems. For this reason, the study of high frequency noise in HBTs constitutes an important feature for the development of these devices and becomes a crucial aspect in system sensitivity for communication applications; for instance, it sets the signal-to-noise level in low-noise amplifiers. In high-speed integrated circuits HBTs operate in the normal active mode, and are typically biased at high current densities (even in quasisaturation) to achieve the largest values of f_T. Due to this fact, high-injection phenomena may occur in the transistor and cause severe degradation in key transistor parameters such as β, transconductance (g_m) and f_T.

Since all the physical properties of the HBT are strongly influenced by the biasing, these high-injection effects can be extremely relevant in the noise performance of the devices and have to be considered carefully in the case of high-frequency low-noise applications. Noise measurements in the gigahertz range require substantial experimental effort, and the optimization of a low-noise device through fabrication and measurement can be very expensive and time consuming. Therefore, to characterize and improve high-speed and low-noise SiGe HBT technology, an adequate modeling of transport based on a microscopic model is of capital importance. The ensemble Monte Carlo (EMC) method yields accurate static results (velocity, current, etc.) under nonequilibrium carrier-lattice conditions (as occurs in a submicrometer base)[3] and also provides the direct calculation of fluctuations in these quantities. The purpose of this work is to perform a microscopic analysis of the noise behavior in an HBT as compared with a BJT with identical geometry and doping levels in emitter-common configuration by means of a two-dimensional (2D) EMC method, thus introducing no assumption about the noise origin.[4] We shall relate the noise sources to the internal mechanisms that control the transport in the devices (band discontinuities, injection level, presence of hot carriers, etc.),[5,6] paying special attention to the different bias conditions in the active mode.

The article is organized as follows. In Sec. II the geometry and doping profiles of the simulated Si BJT and SiGe HBT are presented, together with several details related to the 2D EMC simulator used for the calculations. In Sec. III we report the results of the comparison between the BJT and the HBT for both dc and noise performance. High-injection effects on the dc performance when operating at high bias conditions are described in Sec. III A. In Sec. III B the main features of the frequency dependence of the current spectral densities are reported. Based on the observations of Sec. III A, in Sec III C the bias dependence of the rf base and collector spectral densities is explained, paying special attention to the different regimes of device operation. Finally, Sec. IV summarizes the main conclusions of our work.

[a]Electronic mail: mjmm@gugu.usal.es

 © 2001 American Institute of Physics

Downloaded 23 Jul 2001 to 193.146.202.74. Redistribution subject to AIP license or copyright, see http://ojps.aip.org/japo/japcr.jsp

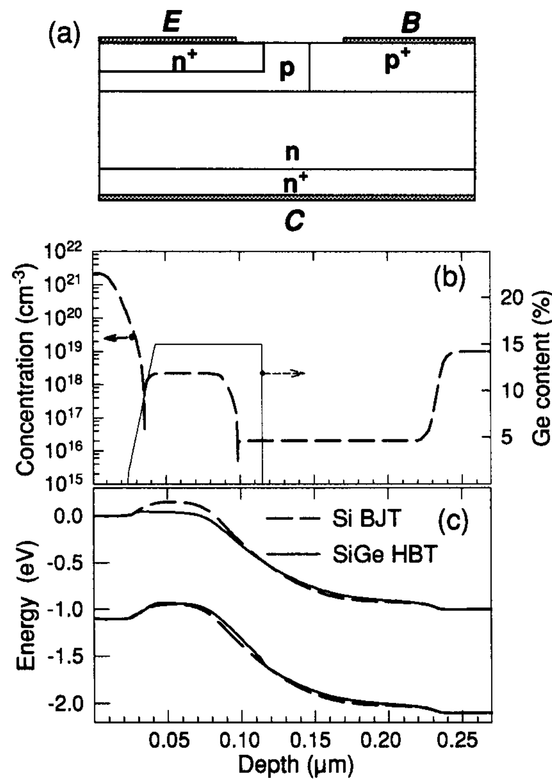

FIG. 1. (a) Geometry of the BJT and HBT. (b) Doping and HBT Ge vertical profiles. (c) Valence and conduction band diagram for the same dc bias conditions in the BJT and HBT.

II. SIMULATED STRUCTURES AND TRANSPORT MODEL

We analyze a Si BJT and a Si-emitter/SiGe-base/Si-collector HBT with identical geometry [Fig. 1(a)] in common-emitter configuration. For the sake of a direct comparison, the vertical doping density (which is identical in both structures) and the HBT Ge profile, both shown in [Fig. 1(b)], are the same as those of the devices analyzed in Ref. 7. The Ge percentage in the HBT has a trapezoidal shape, varying linearly from 0% to 15% Ge in 0.025 μm. The total Ge effective thickness is 90 nm and it is not confined to the metallurgical base. The Si/SiGe heterojunction is located within the collector region at a distance of 15 nm from the base to guarantee a better transistor performance.[7]

For the calculations we use a 2D EMC simulator that is an extension of a previous one-dimensional (1D) version already proved to be a successful tool for bipolar noise studies.[4,5] The microscopic model implemented in the simulator enables one to follow the electron and hole dynamics simultaneously. For electron transport in Si, our EMC simulator considers ellipsoidal and nonparabolic X and L valleys in the conduction band. The character of the conduction band of SiGe remains Si-like up to a Ge molar fraction of 0.85. In the base of the HBT we simulate a SiGe layer grown on a [001] Si substrate under biaxial compressive strain.[4] The strain induces a split in the usually degenerated X-valleys of the conduction band, yielding a strong anisotropy in electron mobility. Both the heavy hole and light hole subbands of the valence band are included in our model. In pseudomorphic layers, an important reduction in the gap is observed, mainly due to an upward shift of the heavy hole subband. Knowledge of the strain-dependent band offsets is critical for obtaining high performance SiGe HBTs. For the handling of the band structure of strained SiGe alloys we followed the work of van de Walle and Martin.[8] The scattering mechanisms considered for electrons and holes are described in Ref. 4.

A variable rectangular mesh (vertical cells ranging from 10 to 25 Å and horizontal cells of 50 Å) locally depending on the doping is used to solve the Poisson equation at time steps of 2.5 fs. The number of simulated particles inside the structure depends on the bias conditions. In the case of the HBT the number of electrons and holes varies respectively from 11 800 and 9000 for $V_{BE}=0.675$ V to 13 900 and 10 300 for $V_{BE}=0.90$ V (both for $V_{CB}=1.0$ V). Similar particle numbers are simulated in the BJT. To deal with the highly doped regions existing in realistic devices, our simulator includes effects such as band gap narrowing, impurity deionization[9] and the Pauli exclusion principle. In order to reduce the computation time, the maximum simulated doping level of the emitter layer takes a value of $3\times10^{19}\,\text{cm}^{-3}$, lower than the real value of $2\times10^{21}\,\text{cm}^{-3}$ reported in Fig. 1(b). This lower doping involves no significant change in the results, since this is just an ohmic region playing no essential role in the device behavior, which is fundamentally controlled by the p-base and the n-collector region. Moreover, the low-field mobility of carriers in Si exhibits a similar behavior for both doping levels. Electron–electron scattering is not included in our simulator since the only influence of this interaction would take place in the nonessential highly doped emitter region close to the contact.

As the purpose of our work is the investigation of the current fluctuations taking place in the devices, an accurate evaluation of the instantaneous bipolar current flowing at each electrode is necessary. To this purpose we employ a technique based on the Ramo–Shockley theorem similar to that used in Ref. 10. This theorem can be applied for bipolar structures and is valid also for an inhomogeneous dielectric medium with an arbitrary fixed charge distribution under time-varying potentials at the electrodes, what makes it useful for the analysis of realistic BJTs and HBTs.[11] According to this theorem, the instantaneous current at an electrode i within the device is given by two components, $I_i(t)=I_i'(t)+I_i''(t)$. $I_i'(t)$ is solely contributed by the movement (under fixed potentials at the electrodes) of the N_e electrons and N_h holes present inside the device

$$I_i'(t)=+\sum_{j=1}^{N_e+N_h} Q_j \nu_j(t)\nabla f_i, \tag{1}$$

where Q_j and ν_j are the charge and the velocity of the j electron or hole superparticle, and f_i is the solution of the Laplace equation $\nabla(\varepsilon\nabla f_i)=0$ under the following conditions: a unit voltage is applied to electrode i, all other electrodes are grounded and all charges are removed from the device. $I_i''(t)$ is the current induced through capacitive coupling between electrodes in the presence of time-varying applied voltages.

From the values of the instantaneous current densities at each electrode provided by the EMC simulator we evaluate

Downloaded 23 Jul 2001 to 193.146.202.74. Redistribution subject to AIP license or copyright, see http://ojps.aip.org/japo/japcr.jsp

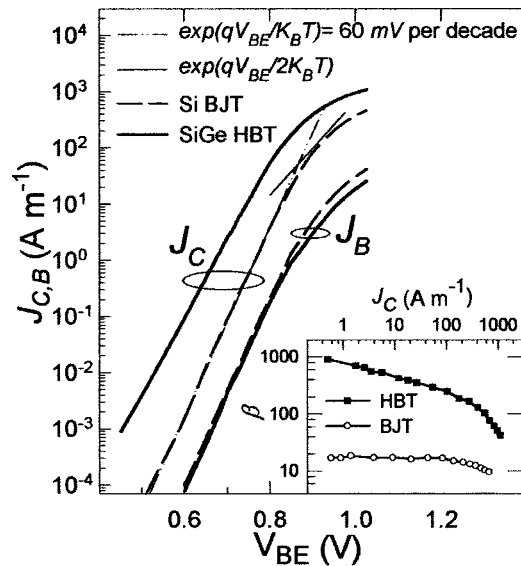

FIG. 2. Simulated base and collector current densities (J_B and J_C) as a function of V_{BE} for $V_{CB}=1.0$ V in the Si BJT and SiGe HBT. The inset shows the current gain β vs J_C in both structures.

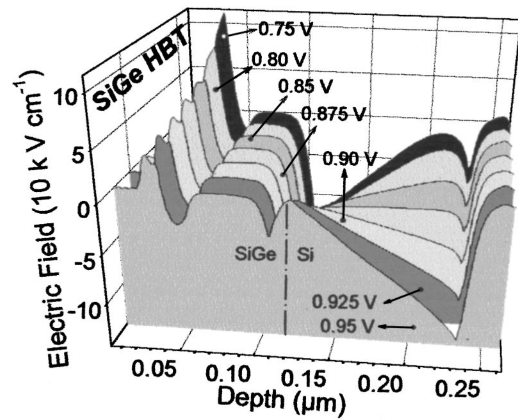

FIG. 3. Electric field from the emitter to the collector in the HBT as a function of the V_{BE} bias for $V_{CB}=1.0$ V. The different plots are shifted to allow a perspective view.

the spectral densities of a single electrode i (emitter, base or collector) current fluctuations (S_{Ji}) together with the cross-correlation spectra of pairs (i and j) of these quantities ($S_{J_iJ_j}$), which are given by

$$S_{J_i}=2\int_{-\infty}^{\infty}\overline{\delta J_i(0)\,\delta J_i(t)}e^{j2\pi ft}dt=4\int_{0}^{\infty}C_{J_i}(t)\cos(2\pi ft)\,dt, \tag{2}$$

$$S_{J_iJ_j}=2\int_{-\infty}^{\infty}\overline{\delta J_i(0)\,\delta J_j(t)}e^{j2\pi ft}dt$$
$$=2\int_{-\infty}^{\infty}C_{J_iJ_j}(t)\cos(2\pi ft)\,dt$$
$$+j2\int_{-\infty}^{\infty}C_{J_iJ_j}(t)\mathrm{sen}(2\pi ft)\,dt, \tag{3}$$

where $\delta J_i(t)=J_i(t)-\overline{J}_i$ (the upper bar indicates time average), and C_{J_i}, $C_{J_iJ_j}$ are autocorrelation and cross-correlation functions of current fluctuations, respectively. S_{J_i} and $S_{J_iJ_j}$ will be used to analyze and compare the noise behavior of the BJT and HBT.

III. RESULTS

A. dc analysis

The base, J_B, and collector, J_C, current densities in the BJT and HBT are shown in Fig. 2 as a function of V_{BE} for $V_{CB}=1.0$ V. The Monte Carlo simulation is not able to provide reliable values of the current for values of V_{BE} lower than those reported in the figure due to the lack of statistical resolution in the presence of a high emitter-base (EB) barrier, as already discussed in the case of other barrier-controlled devices, like Schottky diodes.[12,13] Anyway, the range of V_{BE} where these devices are typically biased corresponds to that reported in Fig. 2. The currents in the simulated devices show an analogous behavior to that found experimentally in similar structures.[7] At *low bias conditions*, when low-level injection prevails, J_B and J_C (except in the HBT) increase exponentially with bias as $\exp(qV_{BE}/K_BT)$, where K_B is the Boltzmann constant and T corresponds to room temperature. The reduction in the base band gap of the SiGe HBT lowers the potential barrier for electron injection from the emitter into the base with respect to that of the BJT [Fig. 1(c)], thus exponentially increasing the number of injected electrons for a given bias. This fact is manifested by the $J_{C,\mathrm{HBT}}/J_{C,\mathrm{BJT}}$ ratio for the same value of V_{BE}, which evidences the *heterojunction effect*. The more effective confinement of holes in the HBT base slightly reduces the flow of holes injected into the emitter, and thus $J_{B,\mathrm{HBT}}$ is slightly lower than $J_{B,\mathrm{BJT}}$ for a given V_{BE}. For a HBT with a flat Ge profile, the movement of the edge of the EB space-charge region (SCR) typically has a small influence on J_C (inverse Early effect). However, as can be seen in Fig. 2, in the trapezoidal Ge HBT J_C does not follow the slope of 60 mV per decade (at room temperature) typical of a ''pure barrier-controlled regime'' found in the Si BJT. A decrease in the slope of J_C with increasing V_{BE} is observed. This effect was theoretically called Ge-ramp effect: the movement of the edge of the SCR in the base typically has an effect on J_C, as emphasized by Crabbé *et al.*[14] Thus, in this range, a bias-independent constant current gain, β, is found in the BJT, while, being significantly higher, β decreases with J_C in the HBT (Fig. 2, inset).

To illustrate the features of transport inside the devices, Figs. 3 and 4 show the vertical profile of the electric field and carrier concentration, respectively, for different bias conditions, both calculated under the emitter electrode in the HBT. It can be observed how, at low $J_C(V_{BE}=0.75\text{ V})$, the field in the collector-base (CB) region has the expected triangular shape reaching an extreme negative value located close to the metallurgical base-collector junction ($\approx$0.11 μm). Since the CB junction is reverse biased, any incident electron that impinge upon its edges is quickly swept across to the opposite region (buried collector) by the CB electric field. Since the CB junction is reverse biased, any incident electron that impinge upon its edges is quickly swept across to the opposite region (buried collector) by the CB electric field. For *low injection* conditions the electron density in the collector depletion region is significantly smaller than the background

Downloaded 23 Jul 2001 to 193.146.202.74. Redistribution subject to AIP license or copyright, see http://ojps.aip.org/japo/japcr.jsp

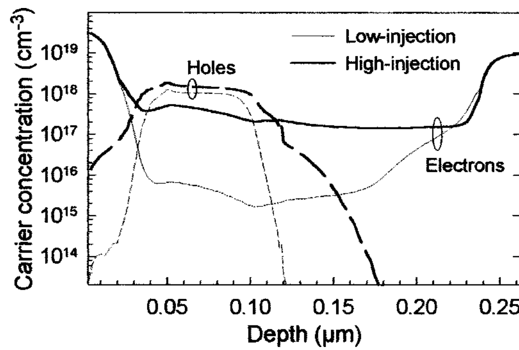

FIG. 4. Electron and hole concentrations in the region localized under the emitter in the HBT under *low-* ($J_C = 10\ \mathrm{A\ m^{-1}}$, thin lines) and *high-injection* conditions ($J_C = 530\ \mathrm{A\ m^{-1}}$, thick lines).

donor or acceptor density, and the CB SCR is not perturbed to a significant extent by the presence of these carriers (Fig. 4).

As V_{BE} increases, a deviation of J_C from the low-bias condition occurs in both transistors (Fig. 2). Different effects can be the origin of this deviation, like the reduction in the forward bias voltage due to lateral ohmic drop in the base or vertical ohmic drop in the emitter. *High-level injection* at the EB junction[15] takes place when the injected minority carrier concentration level in the neutral base increases, becomes comparable to, and even exceeds the doping impurity concentration, being sufficient to induce an increase in the population of the base majority carriers. The low-level injection in the base is assumed to break down (threshold condition) when the electron concentration in the quasineutral base is about 10% of the majority carrier concentration. This high-level threshold voltage, V_{BE-hl}, is equal to 0.92 V in the BJT and 0.83 V in the HBT, both close to the analytical calculation[15] (the conduction band lowering and the aiding quasi-electric field in the EB junction reduces V_{BE-hl} in the HBT). In this regime, as a consequence of the high injection of electrons into the base, the majority carrier concentration (holes) also increases to maintain the quasi-neutrality, as observed in Fig. 4. This effect in turn causes a deviation of the current from the ideal exponential behavior and J_C tends to quasi-saturation as $\exp(qV_{BE}/2K_BT)$ (Fig. 2).[16]

An inspection of the doping profiles in the BJT and HBT reveals that the minimal doping takes place in the collector, close to the base [Fig. 1(b)]. This region serves several useful purposes, like an increase in the breakdown voltage or a reduction of the Early effect, but also other undesirable consequences arise from this low collector doping. As V_{BE} is further increased, the charge density of the minority carriers (electrons) in the space-charge layer may become comparable to the doping density on either one or both sides of the CB junction (Fig. 4), leading to the phenomenon of pushout of the base (or Kirk effect)[17] to the subcollector region, where the doping is sufficiently large to allow the depletion region to form. Its main consequences can be observed in Fig. 3 as V_{BE} increases: a widening of the quasineutral base which penetrates into the collector together with a displacement of the highest fields region towards the subcollector. The onset of this effect takes place for values of J_C around

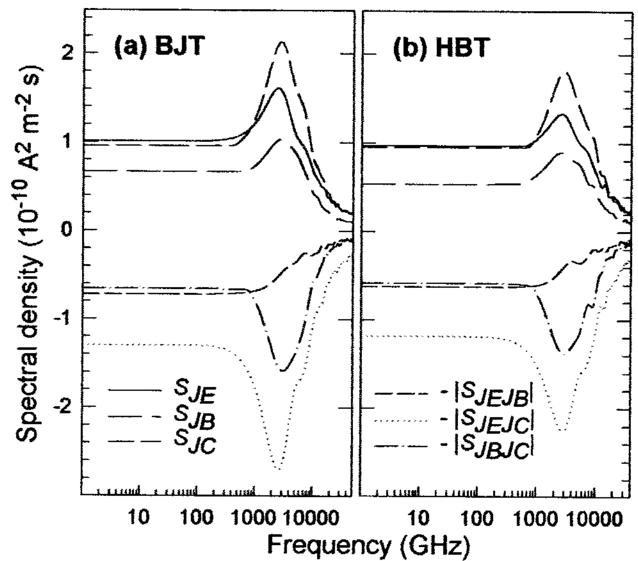

FIG. 5. S_{JE}, S_{JB}, S_{JC}, S_{JEJC}, S_{JBJC}, and S_{JEJB} in (a) the Si BJT and (b) the SiGe HBT for $J_C = 103\ \mathrm{A\ m^{-1}}$.

136 $\mathrm{A\ m^{-1}}$ in the BJT and 107 $\mathrm{A\ m^{-1}}$ in the HBT. At even higher currents, for both structures the field becomes compressed against the boundary between the collector epitaxial region and the buried layer (Fig. 3).

In contrast with the effects of the high-injection in the base, which could be avoided in the HBT by increasing the base doping density, the Kirk effect remains equally important in HBTs and BJTs.[18] These *high-injection* phenomena are largely responsible for the drop in the device performance (β or f_T falloff) at high J_C (Fig. 2, inset) and may have a strong influence on the noise behavior, as will be shown in next sections. Since our purpose is to study the effect of the introduction of Ge in the HBT base on the noise characteristics, maintaining an identical geometry and doping profile as that of the BJT, the benefits induced in the HBT performance by the possibility of increasing the base doping density will not be analyzed.

B. Frequency dependence of spectral densities

The spectral densities as function of frequency are plotted in Figs. 5(a) and 5(b) for the BJT and the HBT, respectively, for an identical J_C (around 100 $\mathrm{A\ m^{-1}}$). The typical noise spectra of these devices exhibit two main ranges as function of frequency. For frequency values lower than the corner frequency, f_C, the most important contribution is $1/f$ noise, while once the frequency surpasses f_C the noise spectra does not show a significant frequency dependence (*white* noise). Our model excludes generation recombination and other mechanisms responsible for $1/f$ noise, which determine the current spectral density in real devices at low frequencies. As observed in Fig. 5, the calculated low-frequency values of S_{J_i} and $S_{J_iJ_j}$ are constant up to frequency values around 150 GHz, well above the disappearance of $1/f$ noise in the device. Therefore, $S_{J_i}(0)$ and $S_{J_iJ_j}(0)$ can be considered as rf values. At very high frequency, a maximum in S_{JE},

Downloaded 23 Jul 2001 to 193.146.202.74. Redistribution subject to AIP license or copyright, see http://ojps.aip.org/japo/japcr.jsp

S_{JB}, and S_{JC} is detected, which is related to the oscillations of space charge at the plasma frequency in the highly doped regions.[4,5,19]

Different reductions in the $S_{J_i}(0)$ and $S_{J_iJ_j}(0)$ terms corresponding to the HBT (right) as compared to those of the BJT (left) are found for the dc condition considered in Fig. 5. As a consequence of the gap of the SiGe base, for identical J_C the base current in the HBT is strongly attenuated (mainly formed by hole injection from the base into the emitter), leading to significant reductions of 17% and 25% in the $S_{JB}(0)$ and $S_{JEJB}(0)$ terms, respectively. A decrease of 10% is also found in $S_{JEJC}(0)$ and in $S_{JBJC}(0)$ in the HBT as compared to the BJT. It is remarkable the strong weight of the $S_{JEJC}(0)$ term in both structures, indicating an effective correlation between emitter and collector noise sources due to the fact that the both are caused by the same electrons. In general, the differences reported here between the several noise terms depend on the bias conditions, as explained in next section.

C. Bias dependence of rf spectral densities

The commonly used noise models of BJTs and HBTs in the microwave frequency range are mainly developed on the basis of the pioneering work of van der Ziel[20] for BJTs. Different models derived from the noise theory of the BJT have been recently developed and proposed in the literature, based on the T or hybrid-π representation of the small-signal equivalent circuit, and extended by the inclusion of different noise sources.[21,22] Usually two intrinsic shot-noise sources resulting from the EB and CB junctions are included, and the addition of a thermal noise source related to the base resistance is also generally needed.[23] These models can be easily implemented in commercial CAD software in order to extrapolate the noise performance up to the millimeter frequency range. In general, the noise behavior of a linear noisy BJT or HBT can be accurately represented as a noiseless two-port circuit defined by its admittance matrix, combined with two noise current generators at the input and output, S_{JB} and S_{JC}, respectively (which can be expressed as function of the different internal noise sources and equivalent-circuit elements),[22] which can be correlated (S_{JBJC}).[21,22,24] The resulting practical noise description of the HBT (noise resistance, minimum noise figure, etc.) can be calculated in terms of the Y parameters and the noise currents using the correlation matrix method.[22] However, some of the noise sources usually included in the models are not very well known (specially their correlation) and typically they are assumed to be of thermal- or shot-noise type.[21,23,24]

Our EMC simulation can provide valuable information about the $S_{JB}(0)$, $S_{JC}(0)$, and $S_{JBJC}(0)$ terms. The rf values of these spectral densities are strongly related to the internal mechanisms controlling the device behavior (band discontinuities, injection level inside the devices, presence of hot carriers, etc.).[5,6] In this section we shall focus on their physical origin, paying special attention to the different injection conditions. Figures 6(a) and 6(b) report the comparison of $S_{JB}(0)$, $S_{JC}(0)$, and $|S_{JBJC}(0)|$ in the BJT and HBT as a function of J_C for a fixed frequency (2 GHz) in the low-frequency plateau. To better illustrate the differences between both devices under high-injection conditions, Figs. 7(a) and 7(b) show the electric field and electron energy vertical profiles from the emitter to the collector for identical J_C (equal to 530 A m^{-1}).

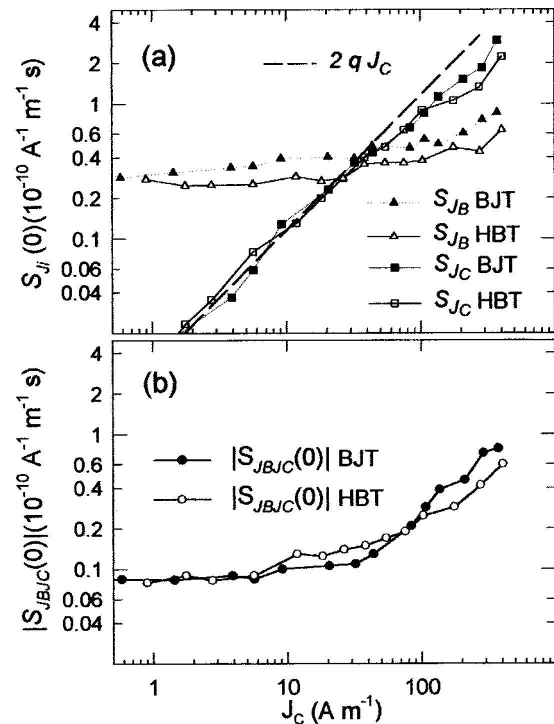

FIG. 6. Comparison of $S_{JC}(0)$, $S_{JB}(0)$, and $|S_{JBJC}(0)|$ in the Si BJT and SiGe HBT. $V_{CB}=1.0$ V, J_C varies with V_{BE}. We find that $|S_{JBJC}|$ essentially coincides with $-\mathrm{Re}\, S_{JBJC}$ in the frequency range of interest, where $\mathrm{Im}\, S_{JBJC}$ is negligible.

Two well-defined different regimes are observed in $S_{JB}(0)$ [Fig. 6(a), circles]. First, for J_C lower than 20 A m^{-1} (low-injection level), we notice that $S_{JB}(0)$ does not undergo

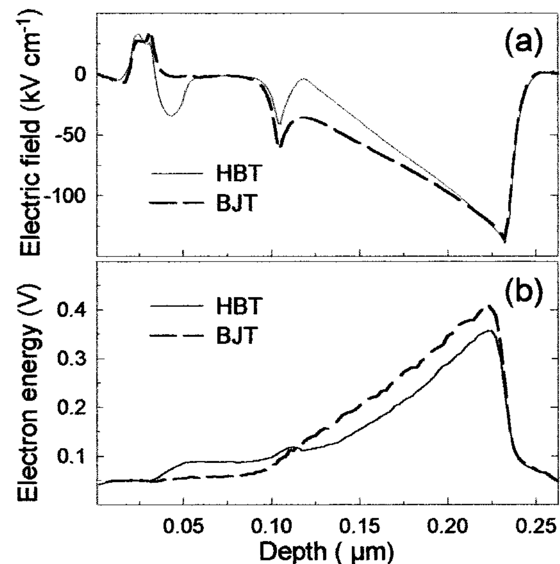

FIG. 7. Comparison of (a) electric field and (b) energy profiles from the emitter to the collector in the BJT and HBT for identical collector current density ($J_C=530$ A m^{-1}) corresponding to high-injection conditions.

Downloaded 23 Jul 2001 to 193.146.202.74. Redistribution subject to AIP license or copyright, see http://ojps.aip.org/japo/japcr.jsp

a strong variation with the dc point in both structures. This indicates that this component is strongly governed by the thermal noise related to the base resistance. We confirm that the presence of an heterojunction does not imply distinguishing aspects in the operation of the HBT under low-injection conditions.[16] The same conclusion was attained in a 1D study of Si/SiGe heterojunctions.[25] For the highest values of J_C, and once the EB barrier plays a minor role, $S_{\mathrm{JB}}(0)$ rises with J_C, and therefore also with J_B, but never reaching a pure shot-noise behavior $(2qJ_B)$ because the thermal component related to the base resistance (which accounts for the two-dimensional access of the holes into the base region under the emitter) continues to be essential.[22] Some authors related this noise source with the *shot* noise at the EB junction due to the electrons which recombine with holes inside the neutral base.[26] In transistors with narrow bases like ours recombination is a very rare event and the base current flows mainly because of hole injection from the base into the emitter.[15] Consequently, generation-recombination mechanisms have not been included in the EMC model and $S_{\mathrm{JB}}(0)$ is given essentially by the fluctuations related to the dynamics of holes in their movement from the base towards the emitter.[15] The increase of $S_{\mathrm{JB}}(0)$ with J_C observed under high injection conditions is related to the dependence of the base resistance on J_C, originated by the widening of the quasineutral base due to the Kirk effect. Remarkably, the base spectral density is significantly lower in the HBT with respect to the BJT as J_C increases.

A different response to that observed in $S_{\mathrm{JB}}(0)$ is exhibited by the $S_{\mathrm{JC}}(0)$ term [Fig. 6(a)], quite similar in both structures. The injection conditions strongly govern the behavior of the $S_{\mathrm{JC}}(0)$ and $S_{\mathrm{JBJC}}(0)$ terms. For low J_C values (lower than 100 $\mathrm{A\,m^{-1}}$), $S_{\mathrm{JC}}(0)$ suffers a pronounced increase with J_C, following a typical shot noise dependence $(2qJ_C)$ in both structures. In an intermediate current range (20–100 $\mathrm{A\,m^{-1}}$) the $S_{\mathrm{JBJC}}(0)$ term exhibits values slightly higher in the HBT than in the BJT [Fig. 6(b)], attributed to the fact that nonequilibrium phenomena become important in the HBT base (from 0.03 to 0.115 μm depth). In fact, in Fig. 7, even if it corresponds to high-injection conditions, it is observed that carriers gain a significant energy from the quasi-electric field generated by the band gap-grading of the EB junction; as a consequence, electrons begin to become hot in the HBT for values of J_C lower than in the BJT.

For J_C above 100 $\mathrm{A\,m^{-1}}$, under high-injection conditions, $S_{\mathrm{JC}}(0)$ deviates from the typical *shot* noise response in both devices, as expected when transport is no longer controlled by the presence of a barrier. Simultaneously, for the highest current densities, the $S_{\mathrm{JBJC}}(0)$ term increases strongly, becoming even more significant than $S_{\mathrm{JB}}(0)$ in the overall noise analysis of the HBT. Both effects begin to occur at the current level for the onset of high-injection conditions ($J_C \approx 108\,\mathrm{A\,m^{-1}}$ in the BJT and $J_C \approx 120\,\mathrm{A\,m^{-1}}$ in the HBT) and under the presence of hot carriers. In fact the displacement of the high-field BC region towards the subcollector observed in Fig. 3 (Kirk effect) favors appearance of hot carriers in a wide region of both structures [Fig. 7(b)], enhancing the $S_{\mathrm{JBJC}}(0)$ cross-correlation term due to excess noise.

In SiGe HBTs at low-injection operation the transition from a narrow gap SiGe base layer to the larger band gap Si collector layer is masked by the high fields in the original CB space-charge region (Fig. 3). However, under high injection conditions, and once the push-out of the base is established, a low-field region (near to become a barrier) is formed at the original SiGe/Si heterointerface of the HBT[27] for the highest values of V_{BE}, which of course is absent in the BJT [Fig. 7(a)]. This ''barrier'' could be avoided by gradually decreasing the Ge content in the CB region; however this would lead to an increase in the average Ge content, thereby imposing a film stability constraint. The main consequence of the presence of this ''barrier'' is that it slightly reduces the appearance of hot carriers in the collector region of the HBT (and therefore their contribution to the excess noise) as compared with the BJT, leading to the differences observed in $S_{\mathrm{JC}}(0)$ and $S_{\mathrm{JBJC}}(0)$ between both devices (lower in the HBT) at the highest values of J_C. Figure 7(b) shows clearly how the low values of the electric field at the SiGe/Si heterointerface prevent the electrons in the HBT to further increase their energy (gained as a consequence of the Ge grading in the EB junction) in a wide portion or the collector region. In contrast, the absence of a Ge grading and a SiGe base layer in the BJT avoids the heating of electrons when entering into the base, but leads to a linear increase of electron energy with position in their movement towards the subcollector, reaching higher energy values than in the HBT over a wide collector region [Fig. 7(b)].

Finally, we point that even if the qualitative behavior of the results we have shown is in principle valid only for our particular structures, some aspects concerning $S_{\mathrm{JC}}(0)$ can be readily extended to other realistic BJT or HBT transistors. Hence, at low injection conditions while the current is controlled by the emitter-base barrier, $S_{\mathrm{JC}}(0)$ will exhibit the typical shot-noise response, and once the device behavior is no longer controlled by the barrier, high injection and hot carrier effects will lead $S_{\mathrm{JC}}(0)$ to deviations from $2qJ_C$. Certainly, by modifying the base or collector doping profiles, the onset of these effects would change and the deviation from the shot-noise behavior would take place at different current values. On the other hand, due to the lack of information about the horizontal dimensions available in the literature (for instance regarding the p^+ access region to the base—doping and exact shape—, base and emitter lengths, etc.) the obtained results for $S_{\mathrm{JB}}(0)$ can only be ascribed to our BJT and HBT. In fact, since this noise source is mainly related to the base resistance (related to the two-dimensional movement of holes from the contact base to the internal base), $S_{\mathrm{JB}}(0)$ is expected to slightly change when varying, for instance, the base doping and Ge profile or the basewidth.

IV. CONCLUSIONS

A 2D EMC simulator has been used to analyze and compare the noise behavior of a Si BJT and a Si-emitter/SiGe-base/Si-collector HBT under different injection conditions. We provide the values of the noise sources typically used to characterize the noise in these devices by means of equivalent circuit models. The main difference between both tran-

Downloaded 23 Jul 2001 to 193.146.202.74. Redistribution subject to AIP license or copyright, see http://ojps.aip.org/japo/japcr.jsp

sistors comes from the presence of the heterojunction in the HBT which, as a consequence of the narrow gap of the SiGe base, allows this device to provide a given level of J_C requiring a much lower value of J_B than the BJT, thus exhibiting a reduction of rf current noise, mainly related to the $S_{\rm JB}$ and $S_{\rm JBJC}$ terms.

The behavior of the noise sources is similar in both transistors. $S_{\rm JB}$ is found to be dominated by thermal noise related to the base resistance. In the absence generation-recombination mechanisms, not included in our model, this term does not show shot-noise behavior at any bias. In contrast, the $S_{\rm JC}$ term becomes shot-noise like in a wide range of currents, as usually assumed in circuit models. However, for the highest voltages, under high-injection conditions and when the EB barrier no longer controls J_C in the transistors, a deviation of $S_{\rm JC}$ from the shot-noise behavior due to the onset of hot carriers effects is found. As concerns the correlation between both noise sources, $S_{\rm JBJC}$, not very well known in the literature and typically neglected, we find that it takes significant values in the whole range of currents analyzed and it becomes specially important under high-injection conditions, where it increases notably with J_C, mainly due to the influence of hot-carrier effects in the collector region.

Apart from the reduction of the $S_{\rm JB}$ contribution in the HBT with respect to the BJT, which can be neglected in the overall noise analysis of this transistor, other differences appear between both devices, mainly under or near high-injection conditions, when the effects related to the presence of the heterojunction become more evident in the noise of the devices. Thus, the quasi-electric field generated by the trapezoidal Ge profile at the EB junction and the barrier generated by the heterojunction at the CB SCR once the push-out of the base has taken place, have some effect on the $S_{\rm JC}$ and $S_{\rm JBJC}$ terms, mainly regulating the importance of hot carrier effects on the noise in the transistors.

As future trend of this work we plan to analyze the influence of the different technological parameters (as the tailoring of the Ge profile or base doping) on the dc characteristics and, of course, on the noise behavior of HBTs.

ACKNOWLEDGMENTS

This work has been funded by Research Project No. PB97-1331 from the Dirección General de Enseñanza Superior e Investigación Científica and Research Project No. SA44/99 from the Junta de Castilla y León.

[1] A. Gruhle, H. Kibbel, U. Erben, and E. Kasper, Proc. Dev. Res. Conf. IIA-2, 1993.
[2] H. Dodo, Y. Amamiya, T. Niwa, M. Mamada, S. Tanaka and H. Shimawaki, IEEE MTT-S Int. Microwave Symp. Digs. **2**, 693 (1998).
[3] C. Jacoboni and P. Lugli, *The Monte Carlo Method for Semiconductor Device Simulation* (Springer, Vienna, 1989).
[4] M. J. Martin, D. Pardo, and J. E. Velázquez, J. Appl. Phys. **84**, 5012 (1998).
[5] M. J. Martin, D. Pardo, and J. E. Velázquez, J. Appl. Phys. **79**, 6975 (1996).
[6] J. Mateos, T. González, D. Pardo, and V. Hoël y A. Cappy, IEEE Trans. Electron Devices **47**, 1950 (2000).
[7] M. S. Peter, J. H, Klootwijk, J. W. Slotboom, F. van Rijs, D. Terpstra, and W. B. De Boer, Proc of ESSDERC99, 1999, p. 716.
[8] C. G. van de Walle and R. M. Martin, Phys. Rev. B **34**, 5621 (1986).
[9] S. K. Chun, J. Appl. Phys. **80**, 4773 (1996).
[10] S. Babiker, A. Asenov, N. Cameron, S. P. Beaumont, and J. R. Barker, IEEE Trans. Electron Devices **45**, 1644 (1998).
[11] H. K. Kim, H. S. Min, T. W. Tang, and Y. J. Park, Solid-State Electron. **34**, 1251 (1991).
[12] C. M. Maziar and M. S. Lundstrom, Electron. Lett. **23**, 61 (1987).
[13] M. J. Martin, T. González, D. Pardo, and J. E. Velázquez, Semicond. Sci. Technol. **11**, 380 (1996).
[14] E. F. Crabbé, J. D. Cressler, G. L. Pattyon, J. M. C. Stork, J. H. Comfort, and Y. Y.-C. Sun, IEEE Electron Device Lett. **14**, 193 (1993).
[15] C.-T. Sah, *Fundamentals of Solid State Electronics* (World Scientific, Singapore, 1991).
[16] R. S. Muller and T. I. Kamins, *Device Electronics for Integrated Circuits* (Wiley, New York, 1986).
[17] C. T. Kirk, IEEE Trans. Electron Devices **9**, 163 (1964).
[18] S. Tiwari, *Compound Semiconductor Device Physics* (Academic, Boston, 1992).
[19] L. Varani, L. Reggiani, T. Kuhn, T. González, and D. Pardo, IEEE Trans. Electron Devices **41**, 1916 (1994).
[20] A. V. D. Ziel, Proc. IRE **46**, 1019 (1958).
[21] J. P. Roux, L. Escotte, R. Plana, J. Graffeuil, S. L. Delage, and H. Balnch, IEEE Trans. Microwave Theory Tech. **43**, 293 (1995).
[22] M. Rudoph, R. Doerner, L. Klapproth, and P. Haymann, IEEE Electron Device Lett. **20**, 24 (1999).
[23] R. A. Pucel and U. L. Rohde, IEEE Microwave Guid. Wave Lett. **3**, 35 (1993).
[24] V. Danelon, F. Aniel, P. Corzat, R. Adde, and G. Vernet, Proceedings of ESSDERC99, 1999, pp. 556–559.
[25] M. J. Martin, D. Pardo, and J. E. Velazquez, Semicond. Sci. Technol. **15**, 277 (2000).
[26] L. Escotte, J.-P. Roux, R. Plana, J. Graffeuil, and A. Gruhle, IEEE Trans. Electron Devices **42**, 883 (1995).
[27] A. J. Joseph, J. D. Cressler, D. M. Richey, and G. Niu, IEEE Trans. Electron Devices **46**, 1347 (1999).

Downloaded 23 Jul 2001 to 193.146.202.74. Redistribution subject to AIP license or copyright, see http://ojps.aip.org/japo/japcr.jsp